

A Decorrelating Multiuser Receiver for Transmit-Reference UWB Systems

Quang Hieu Dang, *Student Member, IEEE*, and Alle-Jan van der Veen, *Fellow, IEEE*

Abstract—Transmit-reference (TR) is known as a realistic but low data rate candidate for ultra-wideband (UWB) communication systems. This paper proposes a new TR-UWB scheme that uses a decorrelating receiver to enable higher data rates with only a reasonably small increase in complexity while still maintaining the ease of synchronization of the original. Integrate and dump with oversampling is used to derive an approximate signal processing data model in a multiuser context. An iterative and a blind receiver algorithm are introduced and tested in simulations. Multiple reference delays are used to further improve the system performance similar to the role of multiple antennas in communication systems. The receiver's complexity and other practical issues in transceiver design are also discussed.

Index Terms—Impulse radio, receiver algorithm, signal processing, transmit-reference, ultra-wideband (UWB).

I. INTRODUCTION

SINCE 2002, ultra-wideband (UWB) has received special research interest as a promising technology for high-speed, high-precision, strong penetration short-range wireless communication applications. The fact that impulse radio (IR) UWB transmission uses ultra-short low-power pulses, helps resolve multipath, simplify the receiver's structure and complexity (no analog up/down converter is required), and allows it to co-exist with other traditional "narrow-band" communication systems.

However, there are significant challenges in developing feasible IR-UWB schemes. Typical UWB channels can be as long as 200 ns, and can be characterized by a dense multipath with thousands of components for some NLOS scenarios [3], [4], which greatly increases the complexity of the RAKE receiver that tries to estimate individual channel taps. Sampling an UWB signal at Nyquist rate is not very cost effective in view of its much lower data (symbol) rate, especially when considering the limitations in sampling rates and/or number of quantization levels of current analog-to-digital converter (ADC) technologies. Moreover, catching the ultra-short pulses (with a duration of only a fraction of a nanosecond) requires strict timing synchronization [5]. Nonideal UWB antennas and other frequency-selective effects cause unwanted distortion on the received UWB pulses.

Manuscript received December 15, 2006; revised July 3, 2007. This work was supported in part by NWO-STW under the VICI programme (DTC.5893). This paper was presented in part at the International Conference on Acoustics, Speech, and Signal Processing, (ICASSP), Toulouse, France, 2006 and also at ICASSP 2007, Honolulu, HI, 2007. The associate editor coordinating the review of this manuscript and approving it for publication was Prof. Dennis L. Goeckel.

The authors are with the Department of Electrical Engineering (EEMCS), Delft University of Technology, 2628CD Delft, The Netherlands.

Digital Object Identifier 10.1109/JSTSP.2007.906649

The transmit-reference (TR) scheme, first proposed for UWB in [6] and [7], emerges as a realistic candidate that can effectively deal with these challenges. By transmitting pulses in pairs (or doublets) in which both pulses are distorted by the same channel, and using an autocorrelation receiver, the total energy of the channel is gathered to detect the signal without having to estimate individual channel multipath components. The simple delay (at transmitter), correlation and integration operations (at receiver) ease the timing synchronization requirements [8] and reduce the transceiver's complexity. Already a single sample may be sufficient to detect one data symbol. Other techniques [9], [10] are proposed to further reduce the receiver complexity in TR-UWB schemes by using mono-bit digital ADCs, which allows parallel sampling configurations to avoid the error propagation issue present in serial ADCs.

However, TR-UWB also has some disadvantages. It is often considered a low-data-rate scheme because of implicit assumptions that the pulse spacing D in a doublet should be longer than the channel length T_h to prevent inter-pulse interference (IPI), and the frame period T_f should be chosen such that there is no inter-frame interference (IFI): together this leads to $T_f > 3T_h$. Since both pulses in a doublet go through the same noisy channel, the correlating operation enhances (and colors) the noise, which degrades the bit-error rate (BER) performance. In most TR-UWB schemes, signals are integrated over the full frame or symbol period, which may accumulate noise, especially at the end of the frame (or the tail of the multipath channel) where the signal strength is much weaker or even absent.

Wideband delay lines longer than a few pulse widths are difficult to implement with high accuracy [11]. Therefore, in [12], we have considered a TR-UWB scheme where the pulse spacing D is very short, much shorter than the channel length T_h . However, the frame length T_f was still taken larger than T_h . In [1], we have lifted this assumption and considered $T_f < T_h$, and introduced equalization schemes to remove the IPI and IFI. As a result, the frame rate can be at least three times higher than in the preceding schemes. In [2], we have extended this scheme to a CDMA-like multiuser context.

To improve the tradeoff between energy capture and noise accumulation, various authors have considered oversampling, which means to take multiple samples per frame by speeding up the integrate and dump operation. For example, in [13], oversampling was used in combination with a GLRT receiver—IPI was assumed to be absent. In [14] and [15], the noise problem was reduced by oversampling and optimized combining of weighted samples. However, the scheme did not allow IFI and is hard to generalize to the multiuser case where user signals are not properly aligned. In the present paper, we use oversampling

to get P samples per frame, but all samples are treated in parallel instead of immediately combining them. This helps to resolve the IFI and makes it easier to extend the data model to the multiuser, multiple delay case.

The IFI problem was also considered in [16], where a data model based on second-order Volterra systems is developed for a frame differential UWB system. The algorithm's complexity quickly grows in longer (and more practical) UWB channels and in a multiuser context. Here, we develop a data model in matrix form and propose receiver algorithms exploiting the sparse structure of these matrices, of which the complexity only grows linearly with the channel length.

Finally, in [17], a multiuser system was proposed for TR-UWB, which considers all digital TR, template averaging, etc. This scheme accepts IPI, which also increases the data rate. However, IFI is not considered and perfect frame synchronization is assumed.

In this paper, we develop a multiuser TR-UWB system that admits both IPI and IFI. Users are allowed to transmit signals asynchronously as in CDMA systems [18], [19]. No synchronization is necessary in the analog part of the receiver: it is running data-independent. In the digital part of the receiver, we will assume without loss of generality that the time offset of each user is known up to an integer multiple of the sampling period—the estimation of this offset is outside the scope of the paper.

It is known that the use of multiple antennas facilitates the equalization problem in communication systems. In this paper, we make use of multiple delays between the two pulses in a doublet. This creates a multichannel scenario that has similar effects as multiple antennas and oversampling. Simulation results show that it gives a significant improvement over the single delay case.

The paper is organized as follows. Section II derives, for clarity, a generic data model for the transmission of a single frame, and subsequently for multiple frames, based on approximations of which the validity is analyzed and simulated in Appendix I. The model is extended in Section III to a general model that includes oversampling, multiple delays, and multiple users. Based on these signal processing data models, blind and iterative receiver algorithms are derived in Section IV, and their performance is shown in simulations in Section V. As conclusion, Section VI summarizes some design considerations of the proposed TR-UWB scheme in relation to practical system design.

II. DATA MODEL—PRELIMINARIES

A. Single Frame

To make the model derivation steps easier to follow and to simplify the expressions, we start from a generic transmission of a single frame of duration T_f .

When a UWB pulse $g(t)$ is transmitted through a UWB physical channel $h_p(t)$ of length T_h , the received signal at the antenna's output (possibly after some bandpass/low-pass received filters) will be

$$h(t) = h_p(t) * g(t) * a(t)$$

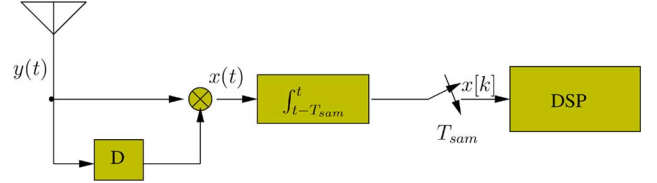


Fig. 1. Autocorrelation receiver.

where $a(t)$ is the antenna response. From now on, $h(t)$ will be regarded as the “composite” channel impulse response.

In TR-UWB systems, pulses are transmitted in pairs (called doublets), one doublet per frame. Within a frame, the first pulse is fixed, while the second pulse, delayed by D seconds, has information in its polarity: $s_0 \in \{-1, +1\}$. The received signal at the antenna output due to one transmitted frame is

$$y_0(t) = h(t) + s_0 \cdot h(t - D).$$

The receiver structure for a single frame is shown in Fig. 1, in which $y_0(t)$ is multiplied with a delayed (by D) version of itself before being integrated and dumped. The sampling period is T_{sam} , and we use oversampling by taking P samples per frame: $T_{\text{sam}} = (T_f/P)$. The resulting signal at the multiplier's output is

$$\begin{aligned} x_0(t) &:= y_0(t)y_0(t - D) \\ &= [h(t) + s_0h(t - D)][h(t - D) + s_0h(t - 2D)] \\ &= [h(t)h(t - D) + h(t - D)h(t - 2D)] \\ &\quad + s_0[h^2(t - D) + h(t)h(t - 2D)]. \end{aligned}$$

Define the channel autocorrelation function as

$$R(\tau, n) = \int_{(n-1)T_{\text{sam}}}^{nT_{\text{sam}}} h(t)h(t - \tau) dt.$$

After integrate-and-dump, the received samples are

$$\begin{aligned} x_0[n] &= \left[R\left(0, n - \frac{D}{T_{\text{sam}}}\right) + R(2D, n) \right] s \\ &\quad + \left[R(D, n) + R\left(D, n - \frac{D}{T_{\text{sam}}}\right) \right]. \end{aligned} \quad (1)$$

In (1), the dominant term is the matched term, $R(0)$, which contains the energy of the channel segments. As shown in Appendix I, the unmatched terms $R(\tau)$ with $\tau \in \{D, 2D\}$ can be ignored if we choose $D > \tau_0$, where τ_0 is a certain correlation length, often very small (less than a nanosecond) for typical UWB channels, and dependent on channel statistics and antenna responses.

The oversampling process (by integrate and dump with $T_{\text{sam}} < T_f \ll T_h$) actually divides the spreading channel into $L_h = \lfloor (T_h/T_{\text{sam}}) \rfloor$ segments (or subchannels). Each segment has its own “channel energy” and “channel autocorrelation function”. The original channel $h(t)$ is now replaced by L_h parameters related to the energy of the channel segments

$$h[n] = \int_{(n-1)T_{\text{sam}}}^{nT_{\text{sam}}} h^2(t) dt \quad n = 1, \dots, L_h. \quad (2)$$

Define the corresponding TR-UWB “channel” vector as

$$\mathbf{h} = [h[1], \dots, h[L_h]]^T. \quad (3)$$

After stacking all discrete samples together in a vector \mathbf{x}_0 and ignoring the cross-terms in (1), we have a generic data model for a single frame as

$$\mathbf{x}_0 = \mathbf{h} \cdot s_0 + \text{noise}. \quad (4)$$

This is a very simple approximate data model for a single frame, based on some statistical properties of the UWB channels and the ultra-wideband nature of the signal and the antennas. As shown later in simulations, this approximation suffers almost no BER performance loss while helps reduce the complexity in data model and receiver algorithms. Based on this generic model, data models for multiple frames, multiple users, and multiple reference delays can be readily derived.

B. Multiple Frames

We extend the preceding model to the transmission of N_f consecutive frames. Each frame has duration T_f , and is assigned a data bit s_j in the polarity of its second pulse, delayed by D from the first pulse. Let us remind that the frame period T_f is much shorter than the channel length T_h so that there always exists IFI. Since a single delay is used for all frames, the receiver structure remains the same as in Fig. 1.

Since we have more than one frame, apart from the matched term and the unmatched terms within every frame, there appears new cross-terms between frames. These cross-terms can also be expressed in terms of the autocorrelation functions of the channel segments. However, the correlation length in the cross-terms are much longer, comparable to the frame length. Therefore, they can be ignored or treated as a noise-like signal.

However, although all the cross-terms can be safely ignored, we still have the matched term that spreads over some next frames because $T_h \gg T_f$. These overlapping parts are IFIs and can be modeled in a channel matrix \mathbf{H} in the data model for multiple frames as

$$\mathbf{x} = \mathbf{H}\mathbf{s} + \text{noise} \quad (5)$$

where \mathbf{x} is the stacking of all received samples, \mathbf{s} is the unknown data vector $\mathbf{s} = [s_1 \dots s_{N_f}]^T$, and \mathbf{H} is the channel matrix that contains shifted versions of the “channel” vector \mathbf{h} in (3). The relation is illustrated in Fig. 2. The IFI effect is also visible in this figure from the fact that many rows in \mathbf{H} have more than one nonzero entry.

We can further improve the accuracy of this data model by including the unmatched terms (with correlation length D) of (1). The improved data model becomes

$$\mathbf{x} = \mathbf{H}\mathbf{s} + \mathbf{B}\mathbf{1} + \text{noise} \quad (6)$$

where \mathbf{B} has the same structure as \mathbf{H} , containing shifted versions of the “unmatched” vector $\mathbf{b} = [b_1, b_2, \dots, b_{L_h}]^T$, where

$$b_n := R(D, n) + R\left(D, n - \frac{D}{T_{\text{sam}}}\right).$$

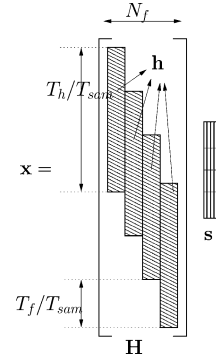


Fig. 2. Data model for multiple frames.

However, as shown later in simulations (Section V-B), little gain is obtained if the model in (6) is used for receiver design, even if D is quite small. Therefore, it is sufficient to use the approximate data model in (5).

C. Effect of Timing Synchronization

UWB communication systems often have stringent requirements on synchronization because of ultra-short pulses. However, in TR-UWB schemes, the analog processing can be kept data-independent as we can easily deal with synchronization issues only after sampling, in the digital domain.

Suppose the full data packet (consisting of multiple frames) is not synchronously sampled, which means that there is an offset G at the beginning of the packet. We can always express the offset as

$$G = G' T_{\text{sam}} + g$$

where G' is an integer and g is a small fraction that satisfies the condition: $0 \leq g < T_{\text{sam}}$.

The integer G' is incorporated in the data model as G' zero padding rows at the top of the channel matrix \mathbf{H} . The offset fraction g causes small changes to the channel vector \mathbf{h} , with entries

$$h[n] = \int_{(n-1)T_{\text{sam}}}^{nT_{\text{sam}}} h^2(t-g) dt, \quad n = 1, \dots, L_h.$$

Since no assumption was made on the unknown channel vector \mathbf{h} , we can still model the whole system as in (5) in the same way as before.

Our receiver algorithms will require G' to be known. If G' is unknown, there are techniques as in [20] that can jointly estimate the unknown offset integer G' and detect the data symbols. In this paper, we will not study in detail these synchronization algorithms.

The implication of the preceding discussion is that by using integrate and dump with oversampling, the proposed TR-UWB scheme is robust against timing errors up to a sampling period. The offset fraction g is absorbed in the unknown channel vector, while the complete synchronization algorithm to estimate the offset integer G' can be implemented in the DSP part, which simplifies the analog part of the receiver.

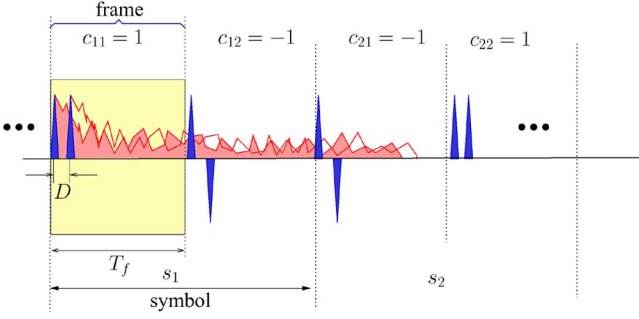


Fig. 3. Pulse sequence structure.

III. DATA MODEL

The preceding preliminary models are extended to the reception of a batch of multiple symbols.

A. Single User, Single Delay

Consider the transmission of a packet of N_s data symbols $\mathbf{s} = [s_1 \dots s_{N_s}]^T$, where each symbol $s_i \in \{+1, -1\}$ is “spread” over N_f frames of duration T_f . The spacing between two pulses in one frame is fixed at D . Each frame is assigned a known user code $c_{ij} \in \{+1, -1\}$, $j = 1, \dots, N_f$. The code varies from frame to frame, and can vary from symbol to symbol similar to the long code concept in CDMA. The receiver still has the simple structure with only one correlator as illustrated in Fig. 1. The structure of the transmitted pulse sequence is illustrated in Fig. 3.

The received signal at the antenna output is

$$y(t) = \sum_{i=1}^{N_s} \sum_{j=1}^{N_f} [h(t - ((i-1)N_c + j-1)N_f T_f) + s_i c_{ij} h(t - ((i-1)N_c + j-1)N_f T_f - D)]$$

where $\mathbf{c}_i = [c_{i1}, \dots, c_{iN_f}]^T$ is the code vector for the i th symbol s_i .

At the multiplier output, the signal $x(t) = y(t)y(t-D)$ will be integrated and dumped at the oversampling rate $P = T_f/T_{\text{sam}}$. Due to uncorrelated channels, as concluded in Appendix I the unmatched terms and the cross-terms can be ignored for the purpose of receiver design. The data model in (5) can be easily extended to include the code c_{ij} . The resulting discrete samples $x[n] = \int_{(n-1)T_{\text{sam}}}^{nT_{\text{sam}}} x(t)dt$, $n = 1, \dots, (N_s N_f - 1)P + T_h/T_{\text{sam}}$ are stacked into a column vector \mathbf{x} , which can be expressed as (see Fig. 4)

$$\mathbf{x} = \mathbf{H} \text{diag}\{\mathbf{c}_1, \dots, \mathbf{c}_{N_s}\} \mathbf{s} + \text{noise} \quad (7)$$

where, as before, \mathbf{H} contains shifted versions of the “channel” vector \mathbf{h} , and the “diag” operator puts the vectors $\mathbf{c}_1, \dots, \mathbf{c}_{N_s}$ into a block-diagonal matrix.

One important result is that the data model in (7) can also be rewritten in another form,

$$\mathbf{x} = \mathcal{C}(\mathbf{I}_{N_s} \otimes \mathbf{h}) \mathbf{s} + \text{noise} \quad (8)$$

where \otimes denotes the Kronecker product and \mathcal{C} is the code matrix of size $((N_f N_s - 1)T_f + T_h)/T_{\text{sam}} \times (T_h N_s)/T_{\text{sam}}$, with entries

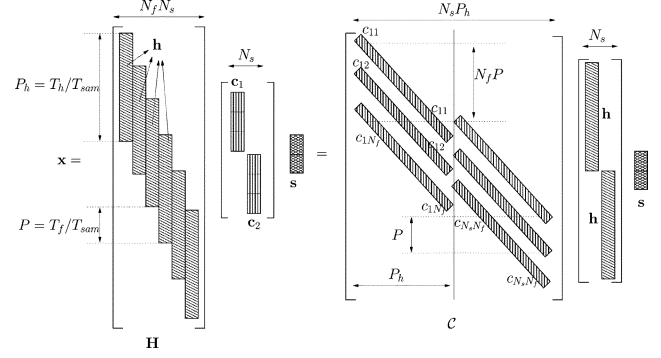


Fig. 4. Data model for the single-user, single-delay case with no offset.

taken from \mathbf{c}_i and structure illustrated in Fig. 4. This form of data model will be used to derive the data model for multiuser, multidelay cases.

B. Multiple Users, Single Delay

Now we derive the data model for an asynchronous multiuser system where the k th user is characterized by a code matrix $[\mathbf{c}_{k1}, \dots, \mathbf{c}_{kN_s}]$, channel vector \mathbf{h}_k , and offset $G_k = G'_k T_{\text{sam}} + g_k$, $0 \leq g_k < T_{\text{sam}}$. The code and the integer G'_k are known, the channel \mathbf{h}_k and g_k are unknown. Since each user goes through a different channel, we can safely assume that two different channels are uncorrelated, which means that all the cross-terms between two users’ channels are noise-like. Therefore, the received signal will be modeled as

$$\begin{aligned} \mathbf{x} &= \sum_{k=1}^K \mathbf{H}_k \text{diag}\{\mathbf{c}_{k1}, \dots, \mathbf{c}_{kN_s}\} \mathbf{s}_k + \text{noise} \\ &= \sum_{k=1}^K \mathbf{C}_k (\mathbf{I} \otimes \mathbf{h}_k) \mathbf{s}_k + \text{noise} \end{aligned}$$

where $\mathbf{H}_k, \mathbf{C}_k$ are the channel matrix and code matrix for the k th user. They have structure as in Fig. 4, except that the time offset G_k shows up as G'_k zero padding rows at the top of the matrices \mathbf{H}_k and \mathbf{C}_k . The effect of the offset fraction g_k is not visible in the model (as discussed earlier in Section II-C, the values of the entries of the channel vector \mathbf{h}_k are slightly changed).

The multiuser data model can be straightforwardly derived as

$$\mathbf{x} = \mathcal{C} \mathcal{H} \mathbf{s} + \text{noise} \quad (9)$$

where $\mathcal{C} = [\mathcal{C}_1 \dots \mathcal{C}_K]$ is the known code matrix; $\mathcal{H} = \text{diag}\{\mathbf{I} \otimes \mathbf{h}_1, \dots, \mathbf{I} \otimes \mathbf{h}_K\}$ is the unknown channel matrix, in which \mathbf{h}_k contains the unknown channel coefficients; and $\mathbf{s} = [s_1^T \dots s_K^T]^T$ contains the unknown source symbols.

C. Multiple Users, Multiple Delays

In the previous sections, we used a fixed delay between the two pulses in a doublet (frame) to simplify the mathematical expressions and the receiver structure. However, the fixed delay will cause spikes at $1/D$ frequency intervals in the spectrum of the received UWB signal, which may conflict with spectral masks. To avoid this problem, the delay between two pulses in a doublet can be made to vary from frame to frame, of which

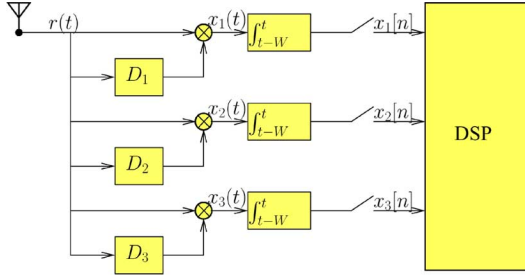


Fig. 5. Receiver structure with multiple correlators.

the pattern is known. From a signal-processing viewpoint, the use of multiple delays will improve equalization and multiuser separation performance, as it improves the conditioning of the matrix \mathcal{CH} by making it taller.

Let the spacing between two pulses in a frame be d_{ij}^k seconds (corresponding to the k th user, i th symbol, j th frame). As before, we choose the delay d_{ij}^k to be very small compared to the frame period and the channel length, i.e., $d_{ij}^k \ll T_f < T_h$. The values of all the delays d_{ij}^k are chosen from a finite set $d_{ij}^k \in \{D_1, D_2, \dots, D_M\}$, of which the pattern is known to the receiver.

At the receiver, we use a bank of correlators, each followed by an “integrate and dump” operator as shown in Fig. 5. The signals at the outputs will be processed in the DSP part of the receiver.

We have M equations corresponding to the M branches of correlators D_1, \dots, D_M . In the single-user case, each equation has a similar expression to (7) and (8)

$$\mathbf{x}^{(m)} = \mathbf{H}^{(m)} \text{diag} \{ \mathbf{c}'_1, \dots, \mathbf{c}'_{N_s} \} \mathbf{s} + \text{noise}, \quad m = 1, \dots, M, \quad (10)$$

where $\mathbf{x}^{(m)}$ is a vector containing the received samples of the m th branch, and $\mathbf{H}^{(m)}$ is similar to \mathbf{H} as before. The code vector \mathbf{c}'_i has entries corresponding to each user, frame and delay. If the delay matches the delay code, the entry contains the corresponding chip value $\{+1, -1\}$, otherwise the entry is 0.

In the data model, we should take into account that all the branches share the same “channel” coefficients \mathbf{h} and the symbol values \mathbf{s} . To this end, we first rewrite the data model of a single branch that corresponds to delay D_m (10) in the “code” by “channel” by “data” form, as

$$\mathbf{x}^{(m)} = \mathcal{C}^{(m)} (\mathbf{I} \otimes \mathbf{h}) \mathbf{s} + \text{noise}, \quad m = 1, \dots, M \quad (11)$$

where $\mathcal{C}^{(m)}$ is a code matrix with structure as before, but with nonzero entries only for frames that have delay codes that match delay D_m .

Now, stacking all received samples in all branches into a column vector, since the channel and source symbols are the same for all branches, the data model for a single-user, multi-delay receiver becomes

$$\mathbf{x} = \mathcal{C} (\mathbf{I} \otimes \mathbf{h}) \mathbf{s} + \text{noise} \quad (12)$$

where

$$\mathcal{C} = \begin{bmatrix} \mathcal{C}^{(1)} \\ \vdots \\ \mathcal{C}^{(M)} \end{bmatrix}.$$

From this equation, the data model for a multiuser, multidelay receiver case can be straightforwardly derived in a similar way as presented in the previous section. The multiuser multidelay data model becomes

$$\begin{aligned} \mathbf{x} &= \begin{bmatrix} \mathcal{C}_1^{(1)} & \dots & \mathcal{C}_K^{(1)} \\ \vdots & \ddots & \vdots \\ \mathcal{C}_1^{(M)} & \dots & \mathcal{C}_K^{(M)} \end{bmatrix} \\ &\times \begin{bmatrix} \mathbf{I} \otimes \mathbf{h}_1 & & \mathbf{0} \\ & \ddots & \\ \mathbf{0} & & \mathbf{I} \otimes \mathbf{h}_K \end{bmatrix} \begin{bmatrix} \mathbf{s}_1 \\ \vdots \\ \mathbf{s}_K \end{bmatrix} \\ &=: \mathcal{CHs} \end{aligned} \quad (13)$$

where $\mathcal{C}_k^{(m)}$ is the code matrix corresponding to the k -user, m th correlator branch. This matrix contains information regarding the user’s chip code, delay code, and time offset.

By using a property of the Kronecker product: $(\mathbf{I} \otimes \mathbf{h}_k) \mathbf{s}_k = (\mathbf{s}_k \otimes \mathbf{I}) \mathbf{h}_k$, the data model above ($\mathbf{x} = \mathcal{CHs}$) can be rewritten in another form ($\mathbf{x} = \mathcal{CSh}$) as

$$\begin{aligned} \mathbf{x} &= \begin{bmatrix} \mathcal{C}_1^{(1)} & \dots & \mathcal{C}_K^{(1)} \\ \vdots & \ddots & \vdots \\ \mathcal{C}_1^{(M)} & \dots & \mathcal{C}_K^{(M)} \end{bmatrix} \\ &\times \begin{bmatrix} \mathbf{s}_1 \otimes \mathbf{I} & & \mathbf{0} \\ & \ddots & \\ \mathbf{0} & & \mathbf{s}_K \otimes \mathbf{I} \end{bmatrix} \begin{bmatrix} \mathbf{h}_1 \\ \vdots \\ \mathbf{h}_K \end{bmatrix} \\ &=: \mathcal{CSh}. \end{aligned} \quad (14)$$

The two forms of the data model in (13) and (14) will be used to derive the iterative algorithms to jointly detect the data symbols and estimate the channel vectors of all users.

D. Remarks

The oversampling included in the integrate and dump process gives us multiple samples per frame. This reduces the individual channel multipath parameters into $L_h = T_h/T_{\text{sam}}$ channel coefficients (corresponding to the energies of the channel segments). The oversampling rate P is a flexible parameter that can be used to improve the performance of the system at the expense of computational complexity.

By introducing multiple delays, we add more diversity to the system. The role of multiple delays is similar to that of multiple antennas in “conventional” communication systems, e.g., CDMA. The difference is that multiple antennas give rise to different channels (more unknown parameters), whereas the bank of multiple delays (in the receiver) shares the same “channel”. In general, the larger the number of possible delays M , the better performance the receiver algorithm can achieve. However, M is limited by constraints on data rate in relation to channel length and channel correlation properties. For example, let τ_0 be the shortest correlation length so that the unmatched

terms can be ignored (cf. Appendix I), then a set of minimal delay values is $\{D_1, \dots, D_M\} = \{\tau_0, 2\tau_0, \dots, M\tau_0\}$. The distance between the last pulse in a frame and the first pulse in the next frame should be larger than $D_M = M\tau_0$. Thus, we should have $T_f > 2M\tau_0$. If the frame length is fixed at T_f , the maximum number of delays will be $M = \lfloor (T_f/2\tau_0) \rfloor$.

IV. RECEIVER ALGORITHMS

A. Alternating Least-Squares Receiver Algorithm

In Section III, we have established linear data models for either the single-user or multiple-users case. In each case, the data model can be expressed in two common forms, as follows:

$$\mathbf{x} = \mathcal{C}\mathcal{H}\mathbf{s} \quad (15)$$

$$\mathbf{x} = \mathcal{C}\mathcal{S}\mathbf{h} \quad (16)$$

where \mathcal{H}, \mathcal{S} are matrices with known structures, constructed from the channel vector \mathbf{h} and source symbols vector \mathbf{s} , respectively. In this equation, \mathbf{x} is the (known) data sample vector, \mathcal{C} is the known code matrix, while \mathbf{s} and \mathbf{h} are the unknowns.

Based on these two forms of the data model, the alternating least squares (ALS) algorithm can be implemented as below.

With an initial channel estimate $\mathbf{h}^{(0)}$, for iteration index $i = 1, 2, \dots$ until convergence

- keeping the channel $\mathbf{h}^{(i-1)}$ fixed, construct the \mathcal{H} matrix, and estimate the source symbols via

$$\mathbf{s}^{(i)} = (\mathcal{C}\mathcal{H})^\dagger \mathbf{x}$$

where $(\cdot)^\dagger$ indicates the Moore-Penrose pseudo-inverse (in this case equal to the left inverse);

- keeping the source symbols $\mathbf{s}^{(i)}$ fixed, construct the \mathcal{S} matrix, and estimate the channel coefficients via

$$\mathbf{h}^{(i)} = (\mathcal{C}\mathcal{S})^\dagger \mathbf{x}.$$

After these iterations, step 1 is repeated once more to get the final estimate of the source symbols. Hard decisions can be used in step 1 to further improve the performance.

Although this is an iterative algorithm that repeatedly uses matrix inversion operations $(\mathcal{C}\mathcal{H})^\dagger$ and $(\mathcal{C}\mathcal{S})^\dagger$, we will discuss in Section IV-D that, by exploiting the sparse structures of these matrices, we can efficiently implement these operations.

B. Initialization—A Blind Algorithm

The ALS algorithm needs an initial channel estimate. As later shown in simulations, the quality of this initial estimate is decisive in the overall performance of the iterative algorithm. Therefore, a fairly good initial estimate of the channel is needed. One idea is that [in view of the definition (2)], the channel vector can be roughly approximated by the channel delay profile. However, in the following, we will introduce a simple blind algorithm, which is similar to the algorithm in [18].

From (13), if the code matrix is tall (this implies the condition $M((N_s N_f - 1)T_f + T_h)/T_{\text{sam}} > K T_h N_s / T_{\text{sam}}$) we can pre-multiply both sides of (13) with the left-inverse of this

known code matrix. The resulting multiuser equation can be decomposed into K single-user equations

$$\mathbf{x}'_k \approx (\mathbf{I} \otimes \mathbf{h}_k) \mathbf{s}_k, \quad k = 1, \dots, K$$

where \mathbf{x}'_k is the k th segment of $\mathbf{x}' = \mathcal{C}^\dagger \mathbf{x}$.

After restacking the vector \mathbf{x}'_k into a matrix \mathbf{X}'_k of size $L_h \times N_s$ as in [18], we have

$$\mathbf{X}'_k \approx \mathbf{h}_k \mathbf{s}_k^T.$$

Subsequently, the channel vector \mathbf{h}_k and the source symbols \mathbf{s}_k of the k th user are found, up to an unknown scaling, by taking a rank-1 approximation of \mathbf{X}'_k . This requires the computation of the SVD of \mathbf{X}'_k and keeping the dominant component.

C. Training-Based Algorithm

In certain cases where the data is transmitted in a long packet, through a channel with fairly constant statistics, we can use a few training symbols to further improve the performance while sacrificing a small portion of the data rate. For example, UWB indoor channels are commonly known to be less varying in time, especially in its channel delay profile which is relevant in our case. With training available, the ALS algorithm is readily adapted. Firstly, based on the known data symbols, we can estimate the channel vector. This estimated channel vector can be used in a zero-forcing receiver to detect the unknown data symbols, etc. It can even be used as the initial channel estimate in the next data packet, which will require no training. This might also help to avoid the local convergence point that may otherwise occur in ALS algorithms.

D. Computational Complexity

The proposed algorithms are all two-step iterations. The complexity of one iteration is derived here. For simplicity of the expressions, we assume that all users have the same parameters and time offsets. As before, $L_h = (T_h/T_{\text{sam}})$ is the channel length in terms of number of samples. Let $L = (T_h/T_f) = (L_h/P)$ be the channel length in terms of frames, assumed an integer number here.

- 1) Given the channel coefficients \mathbf{h} , estimate the source symbols \mathbf{s} by solving $\mathbf{x} = \mathcal{C}\mathcal{H}\mathbf{s}$ (15). This is done by the following steps:

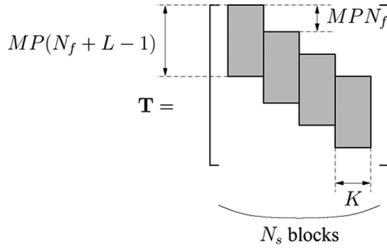
Compute $\mathbf{T} = \mathcal{C}\mathcal{H}$: $KN_s N_f LP$ operations

Compute $\mathbf{y} = \mathbf{T}^H \mathbf{x}$: $KN_s MP(N_f + L)$

Compute $\mathbf{M} = \mathbf{T}^H \mathbf{T}$: $K^2 N_s MP \left(N_f + L + \frac{L^2}{N_f} \right)$

Solve for \mathbf{s} in $\mathbf{M}\mathbf{s} = \mathbf{y}$: $N_s K^3 \left(2 + \frac{L}{N_f} \right)^2$.

In the estimation of the complexities, one can use the fact that \mathbf{T} is a permutation of a block-Sylvester matrix, with structure as shown in Fig. 6. As a result, $\mathbf{M} = \mathbf{T}^H \mathbf{T}$ is a permutation of a block banded matrix, of size $KN_s \times KN_s$, and with bandwidth $B = K[(2 + (L/N_f))]$. This sparsity structure should be exploited when computing \mathbf{M}

Fig. 6. Structure of \mathbf{T} (after permutations).

and when solving for \mathbf{s} via a sparse LU factorization and backsubstitution.

The dominant operation is the computation of \mathbf{M} . Thus, the order of complexity of the estimation of \mathbf{s} is $K^2 N_s MP(N_f + L + (L^2/N_f))$.

- 2) Given \mathbf{s} , estimate the channel coefficients \mathbf{h} by solving $\mathbf{x} = \mathcal{C}\mathbf{S}\mathbf{h}$ (16). This is done by the following steps:

Compute $\mathbf{T} = \mathcal{C}\mathbf{S}$: (only composition)

Compute $\mathbf{y} = \mathbf{T}^H \mathbf{x}$: $KN_s N_f LP$ additions

Compute $\mathbf{M} = \mathbf{T}^H \mathbf{T}$: $K^2 N_s N_f PL^2$ additions

Solve for \mathbf{h} in $\mathbf{M}\mathbf{h} = \mathbf{y}$: $K^2 PL^2$ operations.

In the estimation of the complexities, we used that \mathbf{T} is very sparse with entries $\{0, \pm 1\}$. Each column has only $N_s N_f$ nonzero entries. \mathbf{M} is of size $KLP \times KLP$ and has a multiband structure: only each P th diagonal is nonzero. Consequently, the inversion problem in the last step can be split into P independent inversion problems.

In total, the complexity is $K^2 N_s N_f PL^2$ additions plus $K^2 PL^2$ multiply/additions.

Overall, solving for \mathbf{s} gives the dominant complexity. One iteration thus has a complexity of order $K^2 N_s MP(N_f + L + (L^2/N_f))$ operations. Per estimated symbol per user, the complexity is $KMP(N_f + L + (L^2/N_f))$. Compare this to a single antenna CDMA multiuser decorrelating receiver, which has complexity per user per symbol of order KN_f or LN_f , depending on the type of receiver [19]. The increased complexity (factor MP) is due to the multibranch nature of the TR-UWB receiver structure, and would be similar to the use of multiple antennas.

V. SIMULATIONS

A. Setup

We simulate an asynchronous multiuser TR-UWB system with $K = 3$ equal powered users transmitting Gaussian monocycle pulses of width 0.2 ns. The spacing between two pulses in a doublet may vary in frames, symbols and users, with values taken from the set $\{1, 2, 3, 4\}$ ns. In one user's data packet, we transmit $N_s = 10$ symbols, each symbol consists of $N_f = 10$ frames with duration $T_f = 30$ ns. All the users' symbols and codes are generated randomly. Each user signal is delayed by a random (but known) offset of up to one frame duration, rounded to an integer number of samples. The sampling rate is $T_{\text{sam}} =$

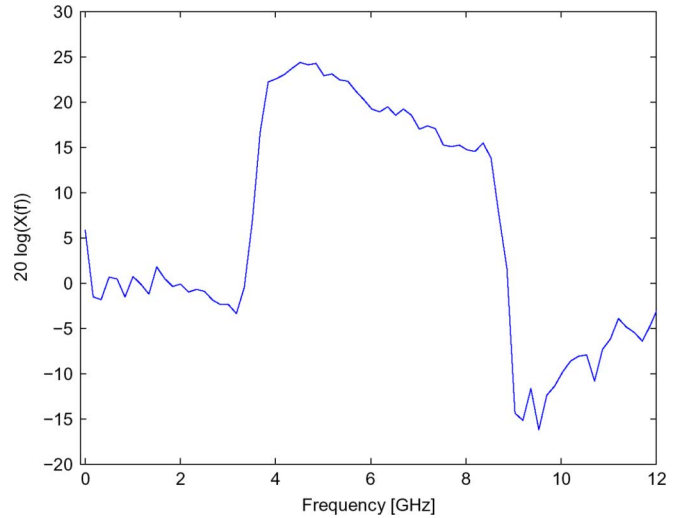


Fig. 7. Frequency response of a practical antenna.

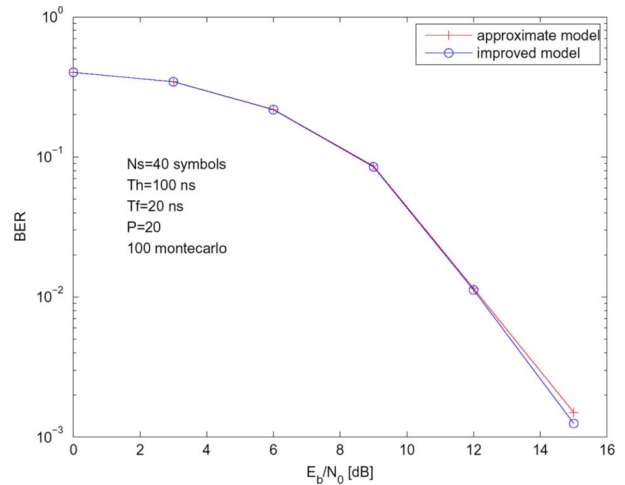


Fig. 8. Comparison of the performance of a ZF receiver based on the approximate data model (5) versus one based on the improved data model (6).

T_f/P and depends on the chosen over-sampling rate, which can be $P \in \{3, 6, 15\}$ samples per frame.

We use the IEEE channel models (CM1, CM2) which are always longer than the frame period, implying that inter-frame interference (IFI) does exist. The non-ideal antenna effect is also included, i.e., a measured antenna response is convolved with the channel and the pulse. The frequency response of the antenna is shown in Fig. 7 [21]. The energy of the resulting channel is normalized to $\int_0^\infty h(t)^2 dt = 1$.

Monte Carlo runs are used to compare the BER versus signal-to-noise ratio (SNR) and channel mean-squared error (MSE) versus SNR plots between various algorithms under different situations. A reference curve for the BER versus SNR plot is the performance of the zero-forcing receiver when the channel coefficients are completely known. Here, SNR is defined as the pulse energy spread by a normalized channel over the noise spectral density, and channel MSE is defined as the mean squared error of the estimate of the "channel" vector \mathbf{h} , i.e., the average of $\|\hat{\mathbf{h}} - \mathbf{h}\|^2$.

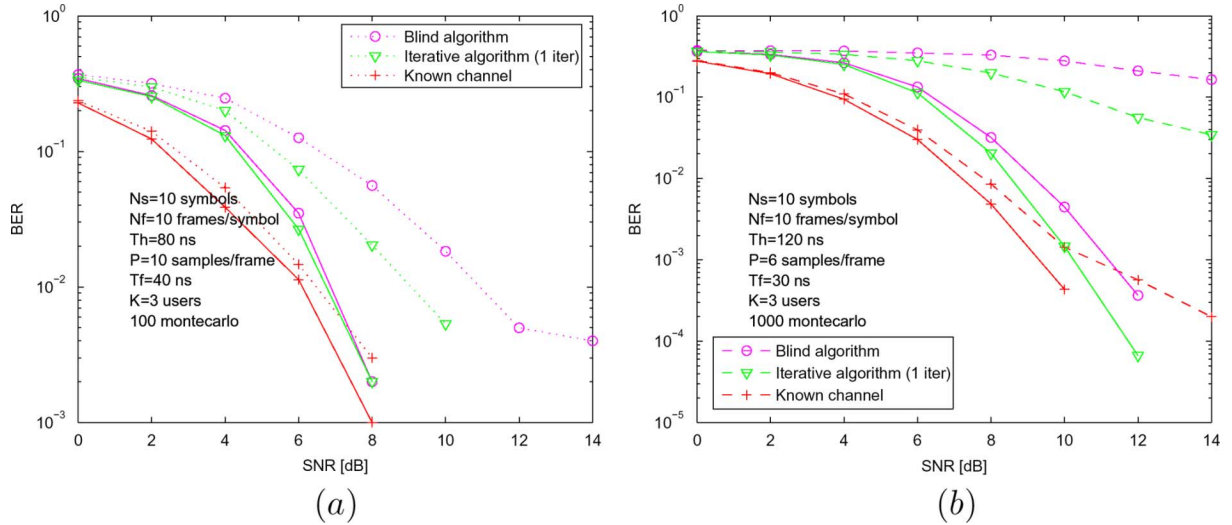


Fig. 9. BER versus SNR performance comparison between single delay and multidelay schemes for (a) CM1, and (b) CM2.

With the parameters given above, one iteration in the iterative algorithm for CM2 case has the complexity of order $K^2 N_s M P (N_f + L + (L^2/N_f)) = 3^2 \cdot 10 \cdot 4 \cdot 6 \cdot (10 + 4 + 4^2/10) = 33696$ operations.

B. The Accuracy of the Data Model

In Section II-B, we have shown two data models: one where all cross-terms due to non-matching delays were ignored (5), and one where cross-terms over a distance D were incorporated (6). In Appendix I, we have analytical and simulated results to show that the unmatched terms are very small compared to matched terms at a certain correlation length $\tau > \tau_0$. In this section, we will indirectly check whether that approximation is sufficient by comparing the BER performance for the zero-forcing receiver when the channel coefficients are completely known under two cases: ignoring the unmatched terms ($\hat{\mathbf{s}} = \mathbf{H}^\dagger \mathbf{x}$), and taking the unmatched terms into account ($\hat{\mathbf{s}} = \mathbf{H}^\dagger (\mathbf{x} - \mathbf{B}\mathbf{1})$).

Fig. 8 compares the BER versus SNR plots for the IEEE channel model CM2. It can be seen that although the improved data model has better performance, the gap is negligible. Meanwhile, the approximate data model has less unknowns, thus results in a less complex receiver algorithm. Therefore, we can conclude that it is sufficient to use the approximate data model.

C. Single Delay Versus Multiple Delays

Fig. 9 shows the BER performance gain of the multiple delay scheme (with $M = 4$ different delays in total) compared to the single delay scheme for the IEEE channel models: CM1 and CM2. The solid lines denote the multiple delay case, the dashed lines denote the single delay case. For CM1, the gain can be 2 dB (for the blind algorithm used for initialization) or 4 dB (for the iterative algorithm) at $\text{BER} = 10^{-2}$. The gaps widen as SNR increases. In the CM2 case, the performance difference is even more visible. The same conclusion can be drawn from the MSE versus SNR curves in Fig. 10.

The reason is, similar to multiple antenna communication systems, that by using M correlation banks at the receiver, we can gather more information to help detect the data symbols and

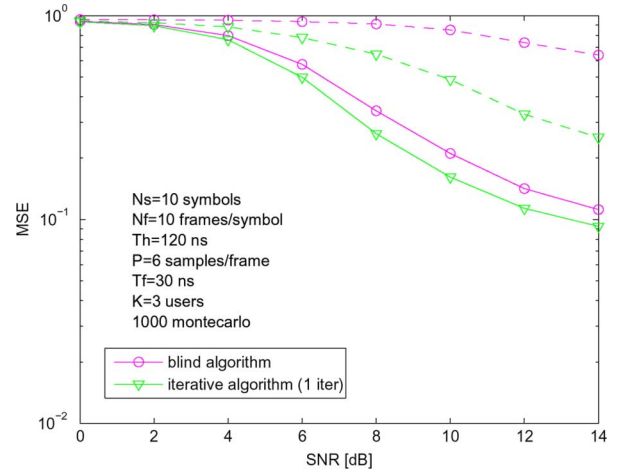


Fig. 10. MSE versus SNR performance comparison between single delay and multidelay schemes for CM2.

estimate the channel coefficients. More specifically, the code matrix \mathbf{C} and the matrices $\mathbf{C}\mathbf{H}$, $\mathbf{C}\mathbf{S}$ are M times taller, which will improve the algorithms' performance and eliminate the BER flooring effect in the high SNR region.

By having $M = 4$ delays, the curves of the blind algorithm can be quite close to the reference curve (ZF receiver with known channel), the difference is only less than 1 dB. The iterative algorithm does not improve much in this case. It will show more improvement under more extreme situations, e.g., when the code matrix \mathbf{C} is wide or barely tall.

It can also be seen that the performance degrades from LOS-CM1 to NLOS-CM2 channel. This is because we keep the same system parameters for both cases (actually the CM2 case has even shorter frame period and lower sampling rate), while the CM2 channel has much longer delay spread, which causes more severe IFI and IPI effects.

From the simulation results in Fig. 9(a) and (b), the iterative algorithm is seen to be only slightly better than the blind algorithm when multiple delays are used. In this specific case, the performance of the blind algorithm is already quite close to the

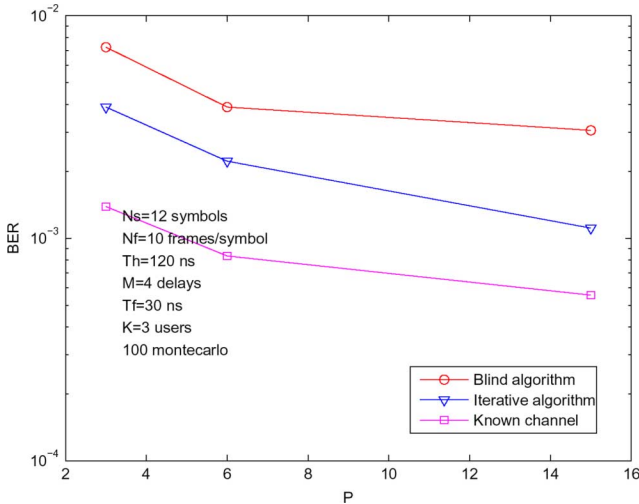


Fig. 11. BER versus P plots for CM2, SNR = 20 dB.

“reference” curve (the gap is less than 1 dB for LOS and 2 dB for NLOS). However, in a more challenging situation where the code matrix \mathbf{C} is barely tall, the improvement will be more visible (as seen in the NLOS case compared to the LOS case).

Note that in Fig. 9, the curve for the known channel (single delay) has a knee at 10 dB. The reason is that even when the channel is known, we only compute the matched terms, i.e., entries of vector \mathbf{h} , and ignore the unmatched terms. For longer channels, i.e., the NLOS case as in Fig. 9(b), it might happen for some random channel realizations that the unmatched terms cause some model error, which is more visible in high SNR region. However, as multiple delays are used, this effect reduces because the matched terms add together while the unmatched terms cancel among themselves. This effect shows up as a better reference curve for multiple delays.

D. BER Versus Oversampling P

Fig. 11 illustrates how the BER performance changes with respect to the oversampling rate $P = 3, 6, 15$ samples per frame at a given SNR value (10 dB). It can be seen that the performance improves as P increases. This is because of the presence of IFI and multiuser interference (MUI) in the system. The more samples per frame, the better we can resolve IFI and MUI. Moreover, it is known that integration over long frame intervals accumulates the noise power in the tail areas of the channel. Therefore, by dividing a frame into more sub-intervals (larger P), we can indirectly deal with the noise problem better by processing the individual subintervals in parallel.

Fig. 11 shows that the BER performance does not increase linearly with P , and there is little gain when $P > 6$, while the frame period is kept fixed at $T_f = 30$ ns. Because P is directly related to the integration period: $T_{\text{sam}} = T_f/P$, the higher the oversampling rate P , the shorter the integration period T_{sam} . As discussed in Appendix I and illustrated in Fig. 13(a) and (b), the model error will increase if we reduce the integration length T_{sam} (or increase P) but at the same time, we gain some IFI/ISI resolving ability (because we have more samples per frame). These effects combined explain the curve in Fig. 11.

VI. TRANSCEIVER DESIGN ISSUES

To conclude the paper, we will take into account some of the implications in this paper for the design of a practical TR-UWB system. What are the constraints on the system parameter values?

A first constraint is posed by the receiver bandwidth, which is limited by spectral masks or antenna design constraints. E.g., the antenna response shown in Fig. 7 has a bandwidth of about 5 GHz. The finite bandwidth determines the correlation distance τ_0 , as discussed in Appendix I. In the receiver algorithm design, we ignored all correlations beyond τ_0 . For the preceding antenna response, we found that we can safely choose $\tau_0 = 1$ ns. Therefore, according to the conclusions in Appendix I.B, the most closely spaced set of possible delays is $\{D_1, \dots, D_M\} = \{1, 2, 3, \dots\}$ ns.

The number of delays M is often constrained by practical considerations: the analog delay lines do take physical space in the receiver, and the receiver algorithm’s complexity increases linearly with M . Therefore, we can often afford only a limited number of delays, say, $M \leq 5$.

Two constraints restrict the choice of the frame size T_f . Firstly, the last pulse of a frame must not overlap with the first pulse of the next frame, even after a maximal delay D_M . Therefore

$$T_f > 2M\tau_0.$$

Secondly, for the blind initialization algorithm described in Section IV-B to work, the code matrix \mathbf{C} must be invertible, hence tall, which implies the condition: $M((N_s N_f - 1)T_f + T_h)/T_{\text{sam}} > K T_h N_s / T_{\text{sam}}$. This can be approximately reduced to

$$M N_f T_f > K T_h.$$

This expression defines a tradeoff between the coding gain (or the symbol period $T_s = N_f T_f$) and the number of users K given the number of delays M and the channel length T_h .

If our aim is to have as high-rate system as possible, then we would set $K = 1$ user, and $N_f = 1$ chips/symbol. The two preceding inequalities give

$$\frac{T_h}{T_f} < M < \frac{1}{2} \frac{T_f}{\tau_0}$$

which leads to

$$T_f > \sqrt{2T_h \tau_0}.$$

This provides a limit on the data rate. For example, if $T_h = 80$ ns and $\tau_0 = 1$ ns, then $T_f > 13$ ns. To have an integer M , we choose T_f a bit larger, e.g., $T_f = 15$ ns corresponding to a data rate of about 66 Mbps. It follows that $M \in \{6, 7\}$.

For a more economic receiver, we would probably take the code length N_f larger. This will lead to a lower data rate, and enables a lower M .

The oversampling rate P can be chosen based on the trade-off between the BER performance (shown in simulations) and the

receiver's complexity (shown in Section IV-D). Computationally, oversampling (P) and multiple delays (M) play almost equivalent roles. Both give rise to a multibranch model. The difference is in the complexity of the analog hardware: oversampling requires faster samplers, whereas multiple delays require more circuitry that runs in parallel. Increasing the code length (N_f) does not cost additional hardware but slows down the data rate and improves the BER performance as usual.

VII. CONCLUSION

In this paper, by oversampling (with multiple samples per frame), we can establish a signal processing data model that includes all the interference terms, i.e., interpulse interference (IPI), interframe interference (IFI), intersymbol interference (ISI), and multiuser interference (MUI). The decorrelating multiuser receiver, followed by an iterative algorithm, can effectively resolve all these interferences without much increase in complexity, which results in a higher data rate compared to other TR-UWB systems. The performance can be further improved by employing multiple reference delays, which simulates multiple antenna systems. The use of oversampling and the structure of the data model imply that the proposed scheme is robust against timing error (up to a sampling period T_{sam}), while a synchronization algorithm (to estimate the unknown offset which is an integer number of T_{sam}) for a similar model was already developed [20]. The problems of imperfect antenna and pulse distortion, and how they affect the system parameters are also addressed. Finally, by allowing to change the oversampling rate P according to the trade-off between performance and complexity, this scheme can be considered as a feasible and flexible bridge between the RAKE scheme (which samples at Nyquist rate) and the "traditional" TR-UWB scheme (which samples at frame/symbol rate).

APPENDIX I CHANNEL STATISTICS

In this section, we will investigate some statistical properties of typical UWB channels (both the measured channel data and the IEEE channel models that include a measured antenna response) to motivate the approximate data models proposed in this paper. In [22], the statistics of pulse distortion due to multipath channel was studied. However, here we focus on the correlation properties only.

In the context of Section II-A, consider the transmission of a single frame by one user, using one delay. The resulting discrete signal (after sampling) at the receiver is

$$\begin{aligned}
 x[n] &= \int_{(n-1)T_{\text{sam}}}^{nT_{\text{sam}}} x(t) dt \\
 &= \int_{(n-1)T_{\text{sam}}}^{nT_{\text{sam}}} h^2(t-D) dt \\
 &\quad + \int_{(n-1)T_{\text{sam}}}^{nT_{\text{sam}}} [h(t)h(t-D) + h(t-D)h(t-2D)] dt \\
 &\quad + \int_{(n-1)T_{\text{sam}}}^{nT_{\text{sam}}} h(t)h(t-2D) dt. \tag{17}
 \end{aligned}$$

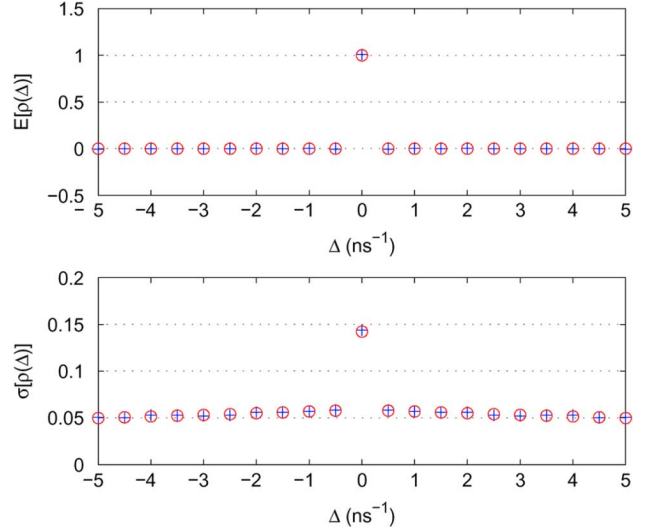


Fig. 12. Statistics of $\rho(\Delta)$ according to the uncorrelated exponentially decaying multipath model, normalized to $E\rho(0) = 1$.

We can see that the first term, the second term, and the third term in (17) are directly related to $\rho(0)$, $\rho(D)$ and $\rho(2D)$, where $\rho(\Delta)$ is the autocorrelation function of the "composite" channel

$$\rho(\Delta) = \int_0^{\infty} h(\tau)h(\tau - \Delta) d\tau. \tag{18}$$

A. Matched Term Versus Unmatched Terms

In [12] (based on more detailed derivations in [23]), we have studied the properties of this autocorrelation function $\rho(\Delta)$ for the UWB multipath channel model with uncorrelated, exponentially decaying channel taps that excludes the antenna response $a(t)$. Fig. 12 shows the analytical and simulated values of the means and variances of $\rho(\Delta)$ for NLOS UWB channel model with RMS delay spread $\tau_{\text{rms}} = 15\text{ns}$ and decay factor $\lambda = 5\text{ns}^{-1}$. It can be concluded that $\rho(\Delta)$ is significant only at $\Delta = 0$, i.e., the matched delay term, while all the mismatched delay terms have zero means and very small variance.

Table I shows the channel correlations for different practical channel measurements [21] that includes a non ideal antenna effect. We can see that as τ increases, $\rho(\tau)$ approaches zeros. So there exists a certain small value τ_0 (about 1 ns) such that $\rho(\tau)$ becomes negligible for $\tau > \tau_0$.

However, since we use oversampling, the integration length T_{sam} is now much shorter, only a fraction of a frame period T_f . Fig. 13 shows the simulated plots to compare the matched delay term and the mismatched delay term (with delay $D = 0.5\text{ns}$) for the IEEE channel models CM1 and CM3, under different sampling rates. The resulting plots are the average over 100 realizations of the UWB channel models including pulse shape and a measured antenna response.

From these plots, we can see that even when oversampling is used, these mismatched terms are so small compared to the matched term that we can omit them, i.e., regard them as noise, in (17). It is also interesting to note that the matched term becomes more dominant when the integration length increases. This is because the matched terms, which are always positive,

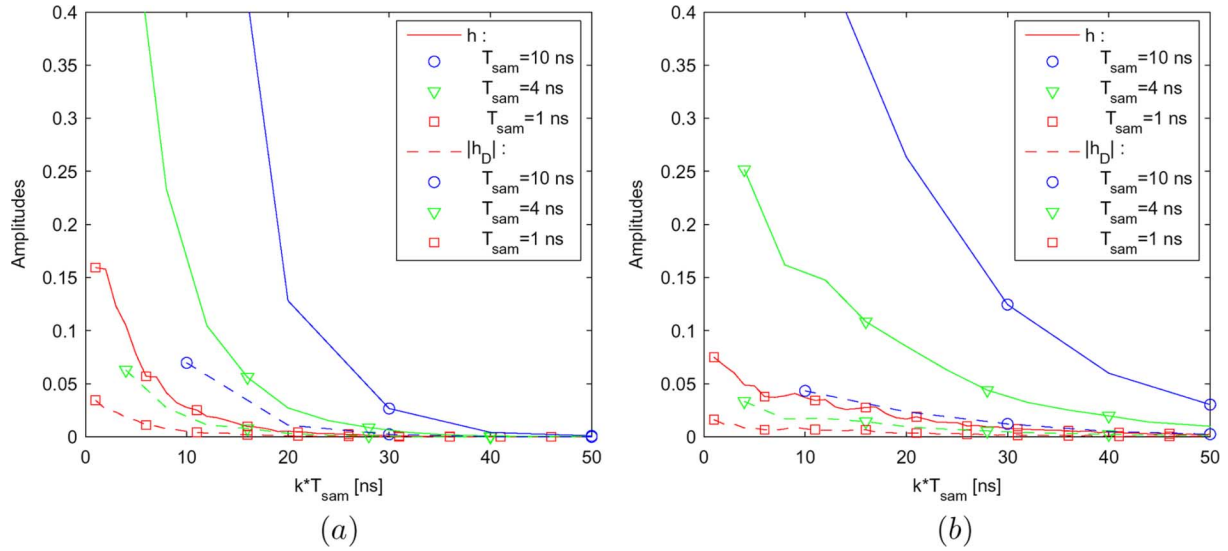


Fig. 13. Matched and unmatched terms for (a) CM1 and (b) CM3.

TABLE I
MEASURED CHANNEL CORRELATIONS $\rho(\tau)$, NORMALIZED TO $\rho(0)$,
FOR SEVEN CHANNEL REALIZATIONS

τ [ns]	0	0.5	1.0	1.5	2.0	2.5
LOS 1	1.000	-0.430	0.236	0.095	-0.100	0.071
LOS 2	1.000	-0.346	0.208	0.183	-0.066	0.076
LOS 3	1.000	-0.380	0.259	0.097	0.036	0.042
LOS 4	1.000	-0.478	0.422	-0.066	0.056	0.031
NLOS 5	1.000	-0.516	0.273	0.053	0.006	0.090
NLOS 6	1.000	-0.376	0.063	0.238	-0.032	-0.100
NLOS 7	1.000	-0.100	0.268	0.115	0.086	-0.071

are added together while the unmatched terms can be either positive or negative. Another reason is that the longer the integration length, the more closely these terms approach the channel autocorrelation function. Therefore, as we reduce the sampling rate, the model error (assuming that the unmatched terms are negligible) will decrease, but at the same time we will lose some IFI resolving ability.

B. Selection of the Delay Values

It is concluded in the previous section that there exist a certain value τ_0 , which is often quite small, such that the channel correlation can be ignored for correlation lengths longer than that value, i.e., $\tau \geq \tau_0$. The value of τ_0 depends mostly on the frequency response of the UWb transmitting and receiving antennas and associated filtering (and partially on the channel statistics).

More specifically, assuming an “ideal” rectangular bandpass frequency response with bandwidth B , centered at frequency f_c , the autocorrelation function has the shape of a modulated squared “sinc” function,

$$R(\tau) = \frac{1}{2B} \cos(2\pi f_c \tau) \text{sinc}(B\tau).$$

Similar to results in filter design theory, the bandwidth defines the width of the main lobe (around the origin) of its envelope before it approaches zero, and the slopes of the frequency response determine how quickly the side lobes approach zero. For the unmatched terms to be small enough to be negligible, the chosen delay(s) should be longer than τ_0 .

From this expression or more visually from its plot, we can find the experimental result of τ_0 as a function of both f_c and B (B is more important because it defines the envelope). The value of τ_0 can be further reduced when the slope of the antenna is designed properly. It is well-known in literature that the raised cosine filter is designed such that its side lobes quickly reduce to zero. Therefore, a raised cosine filter with a roll-off factor $\beta = 1$, and not the “ideal” rectangular shape, is the best candidate in this case.

For multiple delays, there will be unmatched terms when a transmitted doublet with spacing D_i passes through a correlator bank with delay D_j at the receiver, another condition must be satisfied: $|D_i - D_j| \geq \tau_0$ for all $i \neq j$.

These two conditions set the limit of how close two pulses in a doublet can be, and how far the chosen delays should be separated. Obviously, this will directly affect the data rate of the system. Luckily, the value of τ_0 is often very small, less than a nanosecond, and it will decrease as the antenna technology advances.

REFERENCES

- [1] Q. H. Dang and A. J. van der Veen, “Resolving inter-frame interference in a transmit-reference UWb communication system,” in *Proc. Int. Conf. Acoustics, Speech, and Signal Processing (ICASSP)*, Toulouse, France, 2006.
- [2] Q. H. Dang and A. J. van der Veen, “Signal processing model and receiver algorithms for a higher rate multiuser TR-UWb communication system,” in *Proc. Int. Conf. Acoustics, Speech, and Signal Processing (ICASSP)*, Honolulu, HI, 2007.
- [3] D. Cassioli, M. Win, and A. Molisch, “The ultra-wide bandwidth indoor channel: From statistical model to simulations,” *IEEE J. Select. Areas Commun.*, vol. 20, no. 8, pp. 1247–1257, Aug. 2002.
- [4] J. Foerster, Channel Modeling Sub-Committee Report Final IEEE P802.15 Working Group for Wireless Personal Area Networks (WPANs), 2003, Tech. Rep..

- [5] Z. Tian and G. Giannakis, "BER sensitivity to timing offset in ultra wideband communications," in *IEEE Signal Processing Workshop on Signal Processing Advances in Wireless Communications (SPAWC)*, 2003.
- [6] R. Hoctor and H. Tomlinson, "Delay-hopped transmitted-reference RF communications," in *Proc. IEEE Conf. Ultra Wideband Systems and Technologies*, 2002, pp. 265–270.
- [7] J. Choi and W. Stark, "Performance of ultra-wideband communications with suboptimal receivers in multipath channels," *IEEE J. Select. Areas Commun.*, vol. 20, no. 12, pp. 1754–1766, Dec. 2002.
- [8] S. R. Aedudola, S. Vijayakumaran, and T. F. Wong, "Acquisition of direct-sequence transmitted reference ultra-wideband signals," *IEEE J. Select. Areas Commun.*, vol. 24, no. 4, pp. 759–765, Apr. 2006.
- [9] S. Hoyos, B. M. Sadler, and G. R. Arce, "Monobit digital receivers for ultrawideband communications," *IEEE Trans. Wireless Commun.*, vol. 4, no. 4, pp. 1337–1344, Jul. 2005.
- [10] S. Hoyos and B. M. Sadler, "Frequency-domain implementation of the transmitted-reference ultra-wideband receiver," *IEEE Trans. Microwave Theory Tech.*, vol. 54, no. 6, pp. 1745–1753, Jun. 2006.
- [11] S. Bagga, L. Zhang, W. A. Serdijin, J. R. Long, and E. B. Busking, "A quantized analog delay for an IR-UWB quadrature downconversion autocorrelation receiver," in *Proc. IEEE Int. Conf. Ultra Wideband, ICU*, Zurich, Switzerland, Sep. 2005.
- [12] Q. H. Dang, A. J. van der Veen, A. Trindade, and G. Leus, "Signal model and receiver algorithms for a transmit-reference ultra-wideband communication system," *IEEE J. Select. Areas Commun.*, vol. 24, no. 4, pp. 773–779, Apr. 2006.
- [13] S. Franz and U. Mitra, "Generalized UWB transmitted reference systems," *IEEE J. Select. Areas Commun.*, vol. 24, no. 4, pp. 780–786, Apr. 2006.
- [14] G. Leus and A. J. van der Veen, "Noise suppression in UWB transmitted reference system," in *IEEE Signal Processing Workshop on Signal Processing Advances in Wireless Communications, SPAWC*, Lisboa, Portugal, Jul. 2004.
- [15] G. Leus and A. J. van der Veen, "A weighted autocorrelation receiver for transmitted reference ultra wideband communications," in *IEEE Signal Processing Workshop on Signal Processing Advances in Wireless Communications (SPAWC)*, NY, Jun. 2005.
- [16] K. Witrisal, G. Leus, M. Pausini, and C. Krall, "Equivalent system model and equalization of differential impulse radio UWB systems," *IEEE J. Select. Areas Commun.*, vol. 23, no. 9, pp. 1851–1862, Sep. 2005.
- [17] Z. Xu and B. M. Sadler, "Multiuser transmitted reference ultra-wideband communication systems," *IEEE J. Select. Areas Commun.*, vol. 24, no. 4, pp. 766–772, Apr. 2006.
- [18] L. Tong, A.-J. van der Veen, P. Dewilde, and Y. Sung, "Blind decorrelating rake receivers for long-code WCDMA," *IEEE Trans. Signal Process.*, vol. 51, no. 6, pp. 1642–1655, Jun. 2003.
- [19] Q. H. Dang and A. J. van der Veen, "A low-complexity blind multiuser receiver for long-code WCDMA," *EURASIP J. Wireless Comm. Netw.*, vol. 2004, pp. 113–122, Aug. 2004.
- [20] R. Djapic, G. Leus, A. J. van der Veen, and A. Trindade, "Blind synchronization in multiuser transmit-reference UWB systems," in *EU-SIPCO*, Antalya, Turkey, Sep. 2005, Eurasip.
- [21] Z. Irahauten, G. J. M. Janssen, H. Nikookar, A. Yarovoy, and L. P. Ligthart, "UWB channel measurements and results for office and industrial environments," in *Proc. IEEE Int. Conf. Ultra Wideband (ICU)*, Waltham, MA, Sep. 2006, pp. 225–230.
- [22] R. C. Qiu, "A generalized time domain multipath channel and its application in ultra-wideband (UWB) wireless optimal receiver design: System performance analysis," *IEEE Trans. Wireless Commun.*, vol. 5, no. 10, pp. 2685–2695, Oct. 2006.
- [23] K. Witrisal, M. Pausini, and A. Trindade, "Multiuser interference and inter-frame interference in UWB transmitted reference systems," in *Proc. IEEE Conf. Ultra Wideband Systems and Technologies*, Kyoto, Japan, May 2004.



munication (UWB).



applications to wireless communications and radio astronomy

Prof. van der Veen is the recipient of a 1994 and a 1997 IEEE Signal Processing Society (SPS) Young Author paper award, and was an Associate Editor for IEEE TRANSACTIONS ON SIGNAL PROCESSING (1998–2001), chairman of IEEE SPS Signal Processing for Communications Technical Committee (2002–2004), and Editor-in-Chief of IEEE SIGNAL PROCESSING LETTERS (2002–2005). He currently is Editor-in-Chief of IEEE TRANSACTIONS ON SIGNAL PROCESSING, and member-at-large of the Board of Governors of IEEE SPS.

Quang Hieu Dang (S'04) was born in Hai Duong, Vietnam, on October 28, 1976. He received the B.Sc. degree in electronics and telecommunications from Hanoi University of Technology, Hanoi, Vietnam, in 1999, and the M.Sc. degree in 2003 from Delft University of Technology, Delft, The Netherlands, where he is currently pursuing the Ph.D. degree.

From 1999 to 2001, he was a Research and Teaching Assistant at Hanoi University of Technology. His research expertise is on signal processing for long-code WCDMA and for ultra wideband com-

Alle-Jan van der Veen (M'95–SM'03–F'05) was born in The Netherlands in 1966. He received the Ph.D. degree (cum laude) from Delft University of Technology, Delft, The Netherlands, in 1993.

Throughout 1994, he was a postdoctoral scholar at Stanford University, Stanford, CA. At present, he is a Full Professor in the Signal Processing group of DIMES, Delft University of Technology. His research interests are in the general area of system theory applied to signal processing, and in particular algebraic methods for array signal processing, with